Recommended by Amir G Aghdam

Accepted Manuscript

Target Capture and Station Keeping of Fixed Speed Vehicles without Self-Location Information

Samet Güler, Barış Fidan

PII: S0947-3580(17)30464-8
DOI: 10.1016/j.ejcon.2018.06.003
Reference: EJCON 275

To appear in: *European Journal of Control*

Received date: 30 November 2017
Revised date: 19 May 2018
Accepted date: 19 June 2018

Please cite this article as: Samet Güler, Barış Fidan, Target Capture and Station Keeping of Fixed Speed Vehicles without Self-Location Information, *European Journal of Control* (2018), doi: 10.1016/j.ejcon.2018.06.003

Target Capture and Station Keeping of Fixed Speed Vehicles without Self-Location Information

Samet Güler[a], Barış Fidan[b]

[a]Computer, Electrical and Mathematical Sciences and Engineering, King Abdullah University of Science and Technology (KAUST), Saudi Arabia
[b]Department of Mechanical and Mechatronics Engineering, University of Waterloo, Canada

Abstract

Target capture and station keeping problems for an autonomous vehicle agent have been studied in the literature for the cases where the position of the agent can be measured. Station keeping refers to moving the agent to a target whose distances are predefined from a set of beacons that can be stations or other agents. Here we study the target capture and station keeping problems for a nonholonomic vehicle agent that does not know its location and can measure only distances to the target (to the beacons for station keeping). This sensing limitation corresponds to consideration of unavailability of GPS and odometry in practical UAV settings. For each of the target capture and station keeping problems, we propose a control algorithm that uses only agent-target (agent-beacon for station keeping) range and range rate information. We show the stability and convergence properties of our control algorithms. We verified the performance of our control algorithms by simulations and real time experiments on a ground robot. Our algorithms captured the target in finite time in the experiments. Therefore, our algorithms are efficient in scenarios where GPS is unavailable or target identification by vision algorithms is unreliable but continuous agent-target range measurements are available.

Keywords: Target capture, Station keeping, GPS denied environment, Nonholonomic vehicle

1. Introduction

Target capture, which is also referred to as target docking or target pursuit, is the problem of reaching a target by a mobile autonomous vehicle. This problem has been studied in a collection of recent works, see for example [1], [2], and the references therein. The autonomous vehicle A in the target capture problem can be a mobile ground robot or an unmanned aerial vehicle (UAV) trying to reach a target T. Usually, the target T is a sensor that emits a certain form of signal which can be used by a suitable sensor mounted on A to measure distance. The case where the positions of A and T are both known in the global coordinate frame is the standard target tracking problem and can be solved in various ways. However, these solutions cannot be applied when A can sense the distance to T only but not the (relative) position. Thus, one needs to either utilize the derivative of the distance measurements or estimate the target location on-line to achieve the target capture objective.

For example, [3] derives a continuous-time adaptive localization algorithm to localize T by assuming that mobile agent A's own position in global frame and its distance to the target T at each time instant are available. This algorithm is established to be robust to slow persistent drifts of T and guarantees perfect estimation in case of persistence of excitation (PE) of the motion trajectory of A with respect to T. Further, [4] derives a least-squares (LS) based estimation algorithm to achieve the same objective, with further extension of the design to be used with time-of-flight (TOF) sensors. Reference [5] presents results on the sensor/beacon placement, which guarantee practical localization of sensors by using the source signals of a network of beacons.

A further problem involving adaptive localization is adaptive target pursuit, capture, or tracking. Reference [2] proposes an adaptive control strategy based on [3] that achieves the target capture task while localizing the target at the same time. Target pursuit and circumnavigation around a target has been studied in some other recent works as well, including [1, 6, 7, 8]. In [1], the authors derive an algorithm that steers a nonholonomic vehicle, by controlling only its angular velocity, to a source to which the vehicle cannot measure its distance, but receives a signal from the source in the form of an unknown function of the distance. Employing extremum seeking and averaging techniques, circumnavigation around the target is achieved in that work. The localization algorithm of [3] and a motion control law are combined in [8] for the same objective, assuming that the range measurement to the target and the vehicle's own position in a reference frame can be measured. Circumnavigation is studied in [6] as well, with the assumption of bearing angle measurement to the target instead of the range measurement.

Here we propose a control algorithm to solve the aforementioned target capture problem when the self-position measurement is not available to the mobile agent. We assume that the vehicle can sense the vehicle-target distance measurements only; i.e., the vehicle does not utilize any other sensor such as GPS, inertial measurement unit (IMU), or camera in the target capture control algorithm. In Section 2, we examine the target capture problem for a nonholonomic vehicle by using a switching-based control law inspired by the control approach described in [9, 10, 11]. The switching between the control rules is based on the range measurement and the range rate sig-

nal. We first present the control law for a general case where the range measurement and its time derivative are available. In Section 3, we study the stability and convergence properties of the proposed control algorithm. In Section 4, we discuss the case of unavailability of range rate information and the use of observer to compensate this case.

Further, in Section 5, we study the station keeping of nonholonomic vehicles, which steers an autonomous vehicle A towards a target location T, which is not known by the vehicle explicitly, but defined by its pre-defined distances to a set of stationary vehicles/sensors $S_1, \ldots, S_N$, which are known by A. This problem has been considered in some works including [12, 13, 14] and has applications in formation acquisition and maintaining of autonomous multi-agent (vehicle/robot) systems as well as wireless network based target localization and tracking. Assuming that $T - S_i$ distances are predefined and that A can sense its distances to S_i, we modify the control law in Section 2 such that A minimizes the difference between $T - S_i$ and $A - S_i$ distances to accomplish the station keeping task asymptotically.

A preliminary version of this work was presented in [19] where switching control algorithms were proposed for the target capture and station keeping problems without real-time implementation. Here, we modify the target capture control algorithm of [19], demonstrating complete stability and convergence analysis, and propose two novel control algorithms for the station keeping problems as well. Since [8, 9, 10, 11] consider the circumnavigation problem, the methodology of this paper greatly differs from [8, 9, 10, 11] in that our purpose is to steer the vehicle to a close vicinity of the target in contrast to circumnavigation problem where the vehicle is desired to orbit around the target with a relatively bigger radius. Furthermore, the angular control law in our algorithm is bounded similar to [22].

We demonstrate the performance of the proposed control algorithms via simulations and experimental tests on a nonholonomic mobile ground robot in Sections 6 and 7. Section 8 presents the conclusions and future directions of the work.

2. Target Capture Problem and Control Design

In this section, we formally define the target capture problem and present our proposed control law to solve this problem for a mobile nonholonomic vehicle, assuming that the range and range-rate measurements are available to the vehicle.

2.1. Problem Definition

Consider a nonholonomic vehicle A with the dynamics

$$[\dot{x}_A,\ \dot{y}_A]^\top = v\,[\cos(\theta),\ \sin(\theta)]^\top, \quad \dot{\theta} = \omega, \tag{1}$$

where $p_A(t) \triangleq [x_A(t),\ y_A(t)]^\top \in \Re^2$ and $\theta(t) \in (-\pi, \pi]$ are the unknown position vector and heading angle of the vehicle in the global coordinate frame, and $u(t) \triangleq [v(t),\ \omega(t)]^\top \in \Re^2$ is the control input of the vehicle with $0 \le v \le \bar{v}$ and $-\bar{\omega} \le \omega \le \bar{\omega}$, with $\bar{v}, \bar{\omega}$ being the maximum linear and angular speeds of the vehicle, respectively. Consider also a target T with unknown

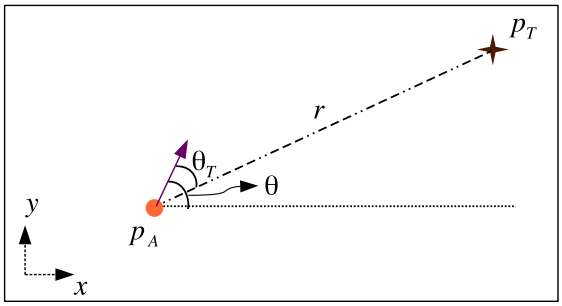

Figure 1: Illustration of the vehicle-target configuration

constant position $p_T \triangleq [x_T,\ y_T]^\top \in \Re^2$. We denote the distance between A and T by

$$r(t) \triangleq \|p_A(t) - p_T\|. \tag{2}$$

This configuration is illustrated in Fig. 1. Another representation of the dynamics (1) uses a time-varying coordinate system centered at A, and the unknown angle $\theta_T \in (-\pi, \pi]$ from the vector $p_T - p_A$ to the current heading of A [9]:

$$\dot{r}(t) = -v(t)\cos(\theta_T(t)), \tag{3}$$

$$\dot{\theta}_T(t) = \omega(t) + \frac{1}{r(t)} v(t)\sin(\theta_T(t)). \tag{4}$$

We focus on driving the nonholonomic vehicle A to the ϵ_r-neighborhood $\mathcal{B}_{\epsilon_r}(p_T) \triangleq \left\{p \in \Re^2 \mid \|p - p_T\| \le \epsilon_r\right\}$ of the target T, where ϵ_r is a pre-defined small threshold constant, and stop the vehicle in this region.

Problem 1. *Consider a nonholonomic vehicle A with motion dynamics* (1)*. Given the range measurement $r(t)$ in* (2) *and its time derivative $\dot{r}(t)$, find a control law $u(t) = [v(t),\ \omega(t)]^\top$ so that A converges to the ϵ_r neighborhood $\mathcal{B}_{\epsilon_r}(p_T)$ of T in finite time.*

A similar problem is considered in [1] in the context of extremum seeking, carrying expense of added sinusoid search signals. Here we follow a more direct approach similar to that of [9, 11] for the target capture problem.

2.2. Control Law

In this subsection, we derive the base control law we propose, assuming that range-rate $\dot{r}(t)$ is perfectly available for measurement. In Section 4, we discuss implementation without having $\dot{r}$ information directly. Inspired by the circumnavigation control design in [9, 11], we propose the control law

$$u = [v,\ \omega]^\top, \tag{5}$$

$$v(t) = \begin{cases} \bar{v}, & \text{if } r(t) > \epsilon_r \\ 0, & \text{otherwise,} \end{cases} \tag{6}$$

$$\omega(t) = \begin{cases} \left((\mathrm{sgn}(\dot{r}(t)) + 1)c + \dfrac{(1+\alpha)\bar{v}}{r(t)}\right)\sigma\left(\dfrac{-\dot{r}(t)}{\bar{v}}\right), & \text{if } r(t) > \epsilon_r \\ 0, & \text{otherwise,} \end{cases} \tag{7}$$

$$\sigma(x) = \begin{cases} 1, & \text{if } x \leq \sqrt{1-\gamma} \\ \frac{1-x^2}{\gamma}, & \text{if } \sqrt{1-\gamma} < x < 1 \\ 0, & \text{if } x \geq 1 \end{cases} \quad (8)$$

where, for $r(t) \geq \epsilon_r$, $\sigma\left(-\dot{r}/\bar{v}\right) = \sigma(\cos(\theta_T))$ is a function that regulates the angle θ_T, $\bar{v}$ is the pre-specified maximum linear speed, and $0 < \gamma < 1$, $c > 0$, and $\alpha > 0$ are design parameters. The plot of $\sigma(\cdot)$ for $\gamma = 0.1$ is provided in Fig. 2. The function sgn is defined such that $\text{sgn}(x) = 1$ for $x > 0$, $\text{sgn}(x) = -1$ for $x < 0$, and $\text{sgn}(0) = 0$. $\alpha > 0$ is a positive constant tuning parameter to be used for vehicle path performance enhancement. Selection of c and α is nominally arbitrary, unless $\bar{\omega}$ is pre-specified, i.e, the asymptotic stability and convergence results to be established in the sequel are valid for any $c > 0$ and $\alpha > 0$. Selection of the values of these parameters for actual implementation is performed via simulation based trials and ad-hoc numerical analysis. The values of c, α, ϵ_r, and $\bar{\omega}$, however, are dependent to each other through the control law (7). (7),(8) imply that

$$0 \leq \omega \leq 2c + \frac{(1+\alpha)\bar{v}}{\epsilon_r}.$$

Hence, in addition to $\bar{v}$, if $\bar{\omega}$ is also pre-specified, α and c need to satisfy

$$0 < \alpha \leq \frac{\epsilon_r(\bar{\omega} - 2c)}{\bar{v}} - 1. \quad (9)$$

(6) and (7) imply that the vehicle stops when it enters the small disc $\mathcal{B}_{\epsilon_r}(p_T)$ around the target T. Selection of the constant γ is further discussed in Section 3.

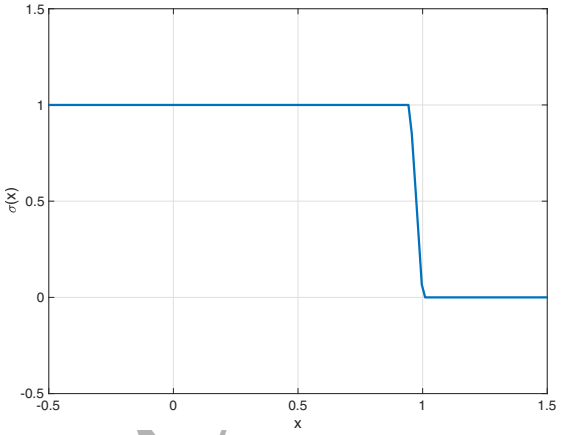

Figure 2: The σ function in (8) for $\gamma = 0.1$.

Remark 1. *In most robotics systems, the linear speed v and angular speed ω are saturated by their maximum values before they are fed to actuators. Our algorithm* (5)-(8) *guarantees that v, ω take values within the bounds $0 \leq v \leq \bar{v}$ and $0 \leq \omega \leq \bar{\omega}$. Furthermore, as will be discussed in the next section, stability and convergence properties of our algorithm do not depend on the vehicle's maximum speeds.*

Remark 2. *For ground vehicle applications, ϵ_r can be chosen small to arrive a close neighborhood of the target, or it can be chosen relatively bigger if the target lies on a foreign vehicle to avoid collision. For fixed-wing UAV applications, since UAV-ground target collision does not occur due to the altitude difference, ϵ_r can be chosen small to move the UAV to a close vicinity of the ground target on the x-y plane.*

3. Stability and Convergence Analysis

In this section we provide stability and convergence analysis of the proposed control law (5)–(8), together with a formal discussion of the intuition behind the selection of switching rules (6),(7). The key component in the control law is the steering ω law (7). The aim is to drive θ_T to zero, corresponding to the direction in which the approach rate $-\dot{r}$ is maximized. This aim can be reformulated as maximizing $\cos(\theta_T)$, which is indirectly measured in terms of $\dot{r}$ and v via (3) as

$$\cos(\theta_T(t)) = \frac{-\dot{r}(t)}{v(t)}. \quad (10)$$

The function $\sigma(\cdot)$ in (8) is used to penalize the deviation of θ_T from its desired value zero, as depicted in Fig. 2. (7) guides the agent A to rotate with a rate dependent on $r(t)$, $v(t) = \bar{v}$, and the sign of $\dot{r}(t)$ as long as A is outside the target vicinity ball $\mathcal{B}_{\epsilon_r}(p_T)$, unless $|\theta_T|$ gets sufficiently close to zero, which is quantified by the term $\sigma(-\dot{r}(t)/\bar{v})$. The switches to zero in the control inputs (6) and (7) prevent chattering and assure that the vehicle stops once it enters the disc $\mathcal{B}_{\epsilon_r}(p_T)$.

To analyze the stability and convergence of the system (3),(4),(6)-(8), we first focus on the motion dynamics for p_A outside of $\mathcal{B}_{\epsilon_r}(p_T)$. For $r(t) \geq \epsilon_r$, substituting (7) into (4) gives

$$\begin{aligned} \dot{\theta}_T = {} & c\left(1 - \text{sgn}(\cos(\theta_T))\right)\sigma(\cos(\theta_T)) \\ & + \frac{\bar{v}}{r}\left((1+\alpha)\sigma(\cos(\theta_T)) + \sin(\theta_T)\right). \end{aligned} \quad (11)$$

The following lemma states some of the stability and convergence properties of (11), treating $r(t)$ as a positive bounded auxiliary signal:

Lemma 1. *For any signal $r(t)$ that satisfies $\epsilon_r < r(t) \leq r_{max}$ $\forall t$, for some finite $r_{max} > 0$,* (11) *has two equilibriums; an isolated equilibrium at $\theta_{e1} = 0$, and an asymptotically stable equilibrium at $\theta_{e2} = -\theta_\epsilon$, where θ_ϵ is defined as*

$$\theta_\epsilon = \sin^{-1}\left(\frac{\gamma}{1+\alpha}\right) < \theta_\gamma = \sin^{-1}\left(\sqrt{\gamma}\right). \quad (12)$$

Furthermore, for (11)*, there exists a finite time instant $t_{r_0} \geq 0$ such that*

$$|\theta_T| \leq \theta_\gamma, \quad \forall t \geq t_{r_0}. \quad (13)$$

Proof. Based on (8), we can write (11) more explicitly, considering the different cases for $\theta_T(t) \in (-\pi, \pi]$:

1. If $|\theta_T(t)| \leq \theta_\gamma$, then:

$$\begin{aligned} \dot{\theta}_T(t) &= \frac{v(t)}{r(t)}\left(\frac{1+\alpha}{\gamma}\sin^2(\theta_T) + \sin(\theta_T)\right) \\ &= \frac{v(t)}{r(t)}\left(\frac{1+\alpha}{\gamma}\sin(\theta_T) + 1\right)\sin(\theta_T), \end{aligned} \quad (14)$$

noting that for $0 < \gamma \ll 1$, we have $0 < \theta_\gamma \ll \frac{\pi}{2}$.

2. If $|\theta_T(t)| > \theta_\gamma$, then:

$$\dot{\theta}_T(t) = c\,(1 - \mathrm{sgn}(\cos(\theta_T))) + \frac{\bar{v}}{r}\,(1 + \alpha + \sin(\theta_T)), \quad (15)$$

since, in this case, $\cos(\theta_T) \leq \sqrt{1 - \sin^2(\theta_\gamma)} = \sqrt{1-\gamma}$. To further analyze (15), Case 2 can be split into the following sub-cases:

2.(a) If $|\theta_T| \geq \frac{\pi}{2}$, then: $\mathrm{sgn}(\cos(\theta_T)) \leq 0$ implies

$$\dot{\theta}_T(t) \geq c + \frac{\bar{v}}{r}\,(1 + \alpha + \sin(\theta_T)) \geq c. \quad (16)$$

2.(b) If $|\theta_T| < \frac{\pi}{2}$, then:

$$\dot{\theta}_T(t) = \frac{\bar{v}}{r}\,(1 + \alpha + \sin(\theta_T)) \geq \frac{\alpha\bar{v}}{r}. \quad (17)$$

(16) and (17) imply that, for Case 2, we have

$$\dot{\theta}_T(t) \geq \min\{c, \frac{\alpha\bar{v}}{r_{max}}\} > 0. \quad (18)$$

For Case 1, analyzing (14), it can be seen that $\dot{\theta}_T = 0$ for $\theta_T \in \{-\theta_\epsilon, 0\}$; $\dot{\theta}_T < 0$ for $\theta_T \in (-\theta_\epsilon, 0)$; $\dot{\theta}_T > 0$ for $\theta_T \in [-\theta_\gamma, -\theta_\epsilon) \cup (0, \theta_\epsilon]$. This, together with (18), proves the lemma. □

We now present the main result of this section.

Proposition 1. *Consider Problem 1 and the control law* (5)-(8). *Then, the vehicle A converges to the disc* $\mathcal{B}_{\epsilon_r}(p_T)$ *in finite time.*

Proof. (3) and (6) imply that $\dot{p}_A = 0$ for $p_A \in \mathcal{B}_{\epsilon_r}(p_T)$. We first show that $r(t)$ is upper bounded, in order to apply Lemma 1. It follows from (14) that if $\theta_T(0) = 0$, then $\theta_T(t) = 0$ for all $t \geq 0$, and hence $\dot{r} = -\bar{v}$ which implies $r(t) \leq r(0)$ for all $t \geq 0$.

If $\theta_T(0) \in (-\frac{\pi}{2}, 0)$, then (3),(17) together with the analysis of Case 1 in the proof of Lemma 1 imply that $\dot{r}(t) \leq 0$ and hence $r(t) \leq r(0)$ for all $t \geq 0$.

Otherwise, (3) implies that $\dot{r}(t) = -\bar{v}\cos(\theta_T(t)) > 0$ only if $|\theta_T(t)| > \frac{\pi}{2}$. Further, (16),(17) together with the analysis of Case 1 in the proof of Lemma 1 imply that $|\theta_T(t)| > \frac{\pi}{2}$ can be satisfied only for a finite time interval of length π/c or less. Hence, $0 < \dot{r}(t) \leq \bar{v}$ only for a finite time interval $t_{f_0} < t < t_{f_1}$. Therefore, $r(t) \leq r(t_{f_1}) < \infty$ for all $t \geq 0$, which completes the proof of boundedness of $r(t)$.

Now, to complete the proof, we only need to show there exists a finite time instant $t_r \geq 0$ such that $r(t_r) \leq \epsilon_r$. To obtain contradiction, assume that

$$r(t) > \epsilon_r, \ \forall t. \quad (19)$$

Based on Lemma 1, this would imply that there exists $t_{r_0} \geq 0$ such that (13) holds. Hence, (3) would imply that

$$\dot{r}(t) \leq -\bar{v}\cos(\theta_\gamma) = -\bar{v}\sqrt{1-\gamma}, \ \forall t \geq t_{r_0}. \quad (20)$$

Taking time integral of (20) leads to

$$r(t) \leq r_{t_{r_0}} - \bar{v}\sqrt{1-\gamma}(t - t_{r_0}), \ \forall t \geq t_{r_0},$$

which contradicts with the assumption (19). Hence, the proof is completed. □

The phase portrait of θ_T is illustrated in Fig. 3. All the solutions starting from the initial condition $\theta_T \neq 0$ converge to $\theta_T = -\theta_\epsilon$.

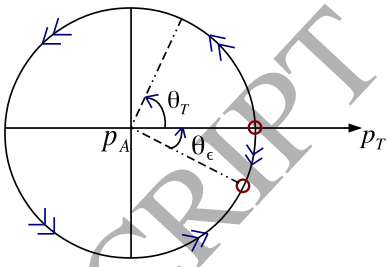

Figure 3: The phase portrait of θ_T: There are two equilibrium points one of which is at $\theta_T = 0$ and the other is at $\theta_T = -\theta_\epsilon$.

Remark 3. *As* γ *tends to zero,* $\sigma(x)$ *becomes sharper around* $x = 1$, *and* θ_ϵ, θ_γ *and* $\theta_{e2} = -\theta_\epsilon$ *tend to zero, which results in faster convergence to the target. As* γ *tends to one,* $\theta_{e2} = -\theta_\epsilon$ *tends to* $\frac{-\pi}{2}$, *which results in slower convergence to the target. However, in real implementations, if* θ_{e2} *is close to zero, the vehicle can miss the equilibrium and* θ_T *can become positive, which can rotate the vehicle one full turn to enter again the zone* $\frac{-\pi}{2} < \theta_T < 0$ *and slow down convergence to the target. We analyze this case in section 7.*

4. Control without Range Rate Information

The control design in Section 2 assumes that the range rate $\dot{r}$ is available. This, in general, is not the case due to sensing limitations of the vehicle A. When the range rate information is not available, one possible attempt is to approximate $\dot{r}$ by taking first-order differences of consecutive r measurement samples. However, this method may yield significantly large approximation errors when the signal-to-noise ratio of the range measurements is low. Typical approaches to obtaining first and higher order derivative estimates of a measured signal include high gain observer and sliding mode observer designs [15]. On the other hand, in [19], a linear first-order filter is applied to approximate the range-rate signal.

[17, 18] develop results for the super twisting algorithm, a special class of the second-order sliding mode observers, for perturbed systems. Motivated by [17, 18], [9] uses a sliding-mode observer to estimate the range-rate from range measurements as follows:

$$\begin{aligned} \dot{\hat{x}}_1(t) &= \hat{x}_2 + k_1|x_1 - \hat{x}_1|^{\frac{1}{2}}\mathrm{sgn}(x_1 - \hat{x}_1), \\ \dot{\hat{x}}_2(t) &= k_2\mathrm{sgn}(x_1 - \hat{x}_1) + k_3(x_1 - \hat{x}_1), \end{aligned} \quad (21)$$

where k_i are design constants, $\mathrm{sgn}(\cdot)$ is as in (8), and $\hat{x}_1$, $\hat{x}_2$ are estimates of the range r and range-rate $\dot{r}$ signals, respectively.

An advantage of employing sliding-mode observer (21) in state estimation is that the estimated signal $\hat{x}_2$ converges to the actual signal $\dot{r}$ in finite time [9].

The sliding-mode observer technique can be applied here together with the control law (5) to solve the target capture problem as well by relaxing the range-rate signal knowledge assumption. In that circumstance, the control law is defined by (5)-(8) with the exception that in (7), $\dot{r}$ is replaced by the estimate $\hat{x}_2$ which is obtained by (21).

5. Range Based Station Keeping

In Section 2, we proposed a target capture control law for a nonholonomic vehicle A for driving A to the target location p_T. There we assumed that A has the vehicle-target distance measurements $r(t)$ all the time. Target capture objective has its own hardness because the self-position is not available to A. In this section, we consider a more challenging scenario: A does not know the target location p_T and the vehicle-target distance $r(t)$; the only information available to A is the set of desired distance values between p_T and each of the other vehicles/sensors in the multi-agent network. The objective of acquiring and maintaining this set of desired distances simultaneously is called *station keeping problem* [16].

Station keeping is as significant as target capture and plays a critical role in formation acquisition in multi-agent systems [20]. However, station keeping problem is more difficult to solve than target capture, especially for nonholonomic vehicles. As will be more clear in the sequel, the difficulty stems from many aspects. First is the unavailability of the vehicle-target distance. This fact prevents the designer from employing tools of classical feedback control and restricts the range of applicable control techniques to a narrow domain. Instead of the vehicle-target distance, the designer is given a set of distance values that nonlinearly depend on the target location, the vehicle's self location as well as the locations of other vehicles/sensors. Furthermore, as is the case for the target capture problem studied in Section 2, position based control algorithms/laws cannot be applied to station keeping problem directly due to the assumption of unavailibility of the vehicle's self-position, and the nonholonomic vehicle kinematics needs to be taken into account. We tackle these issues below by employing the available measurements in the nonlinear control design deliberately.

In the remainder of this section, we define the station keeping problem in general terms and propose our control law comparing it with the results of [12, 13, 16].

5.1. Problem Definition

For convenience of the problem definition and the analysis, we focus on 2-dimensional case. We consider the following problem:

Problem 2. *Consider a* nonholonomic vehicle A *with motion dynamics* (1) *and a set of* N *sensor stations* $\mathcal{S} = \{S_1, \cdots, S_N\}$, $N \geq 3$, *with unknown positions* $p_i \in \Re^2$ *for each* S_i. *Consider also a target location* $p_T \in \Re^2$ *for* A *that is defined in terms of a given set of compatible desired distances* d_i^*, *to satisfy*

$$\|p_T - p_i\| = d_i^*, \ \forall i. \tag{22}$$

Assume that p_i *are not collinear, and the desired distances* d_i^* *and actual distances* $\|p_A(t) - p_i\| \triangleq d_i(t)$ *are available to* A. *Find a control law* $u = [v(t), \ \omega(t)]^\top$ *so that* A *converges to the* ϵ_r *neighborhood of* $\mathcal{B}_{\epsilon_r}(p_T)$ *of the target location* p_T *in a finite time.*

Remark 4. *In order to uniquely specify* p_T *by the distances* d_i^*, *we need* $N \geq 3$ *sensors on a two-dimensional Euclidean plane.*

The configuration of the scenario of Problem 2 is illustrated in Fig. 4.

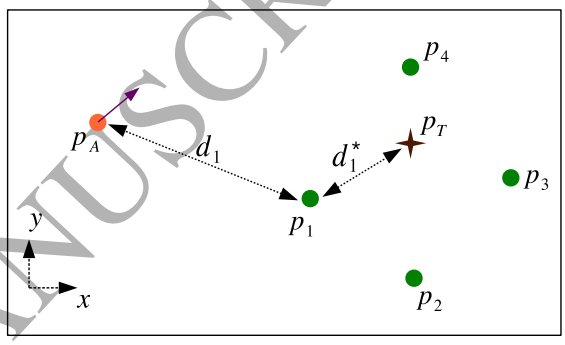

Figure 4: Depiction of the station keeping scenario for a four-sensor case

Problem 2 is defined in the context of sensor networks by assuming that the stationary agents in the network are anchors, i.e., sensors with known positions. In that setting, A is driven to the target p_T whose distances to the set of anchors are available to A, assuming A measures its distances to the anchors at all time. Another interpretation of Problem 2 in the context of robotic networks is as follows: Given a set of N stationary vehicles $\mathcal{S} = \{S_1, \cdots, S_N\}$, $N \geq 3$, with unknown positions $p_i \in \Re^2$, a mobile sensory vehicle A with unknown position $p_A(t) \in \Re^2$ is required to *merge* to $\mathcal{S}$ by converging to a target location p_T which is at a specified distance d_i^* to each vehicle S_i in the network.

Problem 2 has been studied in [12, 13, 16], assuming the mobile vehicle A has holonomic point agent kinematics and the self-position information is available to A, as opposed to what is assumed here. [13] has proposed an adaptive switching control law to solve Problem 2 for the three-sensor case assuming the distance measurements $d_i(t)$ are noisy. [16] has studied the case of $N \geq 3$ sensors in both two and three-dimensional spaces for holonomic vehicles. [16] has proposed an indirect adaptive control method that estimates the unknown sensor positions using the distance measurements $d_i(t)$ and the self position of A, then uses these estimates in a gradient control law applied to a cost function whose unique minimum corresponds to the target location p_T.

We adapt the A-centered polar dynamic representation (3),(4) to the setting of Problem 2 considering the relative location of

each S_i as follows:

$$\dot{d}_i(t) = -v(t)\cos(\theta_i(t)), \tag{23}$$

$$\dot{\theta}_i(t) = \omega(t) + \frac{1}{d_i(t)}v(t)\sin(\theta_i(t)). \tag{24}$$

where $i = \{1, \cdots, N\}$ and $\theta_i \in (-\pi, \pi]$ is the angle from the vector $p_i - p_A$ to the current heading of A. Here, $d_i(t)$ and $\theta_i(t)$ can be considered as the analogue of the range term r and the angle θ_T of the target capture dynamics (3),(4). Note that, defining the unknown distance between A and T as in (2) and the unknown angle $\theta_T \in (-\pi, \pi]$ from the vector $p_T - p_A$ to the current heading of A, as before, the kinematic relations (3), (4) are still valid.

Based on the above observations, we propose three different approaches to Problem 2 in the following subsections.

5.2. Control Design Based on Inter-Vehicle Distance Regulation

The aim of the first approach is to simultaneously drive the individual station distance keeping errors, i.e., the entries of

$$E(t) = [e_1(t), \cdots, e_N(t)]^\top, \quad e_i(t) = d_i(t) - d_i^*, \tag{25}$$

to zero via minimizing a certain norm of $E(t)$. This norm was selected to be a weighted form of the Euclidean norm

$$\|E\|_2 = \left(e_1^2 + \cdots + e_N^2\right)^{1/2}. \tag{26}$$

Alternatively, one can consider the error term $r_E(t)$ to be minimized as the ∞-norm of $E(t)$,

$$r_E(t) = \|E(t)\|_\infty = \max_{i\in\{1,\cdots,N\}} |e_i(t)|, \tag{27}$$

with the maximizer index

$$i_E(t) = \arg\max_{i\in\{1,\cdots,N\}} |e_i(t)|. \tag{28}$$

Lemma 2. *Consider Problem 2. Then, we have $r(t) = \|p_A(t) - p_T\| > r_E(t)$ when $p_A(t) \neq p_T$, where r, r_E are defined in (2),(27), respectively.*

Proof. In each triangle $\triangle p_A p_T p_i$ for $i = 1, \cdots, N$, noting that $\|p_A - p_T\| = r$, $\|p_A - p_i\| = d_i$, $\|p_T - p_i\| = d_i^*$, from the triangle inequality, we have $r + d_i^* \geq d_i$ and $r + d_i \geq d_i^*$. Hence, $r(t) > |e_i(t)|$ for all i and all t, and the result follows. □

We modify the control law derived in Section 2 to solve Problem 2 as follows:

$$u = [v,\ \omega]^\top, \tag{29}$$

where

$$v(t) = \begin{cases} \bar{v}, & \text{if } r_E(t) > \epsilon_r \\ 0, & \text{otherwise,} \end{cases} \tag{30}$$

$$\omega(t) = \begin{cases} \left((\mathrm{sgn}(\dot{d}_{i_E}(t)) + 1)c + \dfrac{(1+\alpha)\bar{v}}{d_{i_E}(t)}\right)\sigma\left(\dfrac{-\dot{d}_{i_E}(t)}{\bar{v}}\right), & \text{if } r_E(t) > \epsilon_r \\ 0, & \text{otherwise.} \end{cases} \tag{31}$$

where the switching function $\sigma(\cdot)$ is defined, as before, in (8), and α, c are as in (9).

5.3. Control Design Based on Circumnavigation

The second approach we propose is to first set the vehicle A on a circular orbit with radius d_i^* around p_i for a particular $i \in \{1, \ldots, N\}$ by utilizing the circumnavigation algorithm in [10] and then stop it, while moving on this orbit, when it arrives at $\mathcal{B}_{\epsilon_r}(p_T)$. Arrival of $\mathcal{B}_{\epsilon_r}(p_T)$ is checked utilizing Lemma 2. The particular i, the index of the station $\mathcal{S}_i$ to orbit around, can be selected based on the a priori information about the sensing and communication reliability, or having the minimal initial distance $d_i(0)$ to A, or having the minimal distance d_i^* to the target T. Hence, the proposed motion algorithm based on [10] is as follows:

$$v(t) = \begin{cases} \bar{v}, & \text{if } r_E(t) > \epsilon_r \\ 0, & \text{otherwise,} \end{cases} \tag{32}$$

$$\omega(t) = \begin{cases} -k\left(\bar{v}\cos\left(\sin^{-1}\left(\dfrac{d_a}{d_i(t)}\right)\right) - \dot{d}_i(t)\right), & \text{if } d_i(t) \geq d_a \\ 0, & \text{otherwise.} \end{cases} \tag{33}$$

where $k > \dfrac{1}{d_i^*}$ is a scalar design constant and $d_a = \sqrt{(d_i^*)^2 - \dfrac{1}{k^2}}$. We now present the convergence result of (32),(33).

Proposition 2. *Consider Problem 2 and the control law (32),(33). Then, the vehicle A converges to the disc $\mathcal{B}_{\epsilon_r}(p_T)$ in finite time.*

Proof. Theorem 3.1 of [10] implies that there exists a finite time instant t^* such that $|e_i(t)| < \epsilon_r$ for $t > t^*$. Since T lies on the circle with center p_i and radius d_i^*, this further implies the convergence to $\mathcal{B}_{\epsilon_r}(p_T)$ in finite time. □

5.4. Control Design Based on Convex Station Keeping Cost

In this section, we propose another alternative approach inspired by the convex station keeping cost approach of [16, 21]. The authors in [21] solve the problem of localization based on range measurements by minimizing a convex cost function that uniquely defines the target point at its only minimum point. The authors in [16] further proposes a controller based on the same cost function to steer the vehicle A to p_T assuming that p_A, together with d_i, d_i^*, are known to A. Both [21] and [16] use the radical axes as the key tool. A radical axis l of two circles $C(p_i, d_i^*)$,$C(p_j, d_j^*)$ has the property that for any q on l, the following holds:

$$\|q - p_i\|^2 - \|q - p_j\|^2 = (d_i^*)^2 - (d_j^*)^2. \tag{34}$$

If p_A is at distance δ_{ij} from l at the p_i side (without loss of generality), we have (Fig. 5):

$$\begin{aligned} d_i^2 - d_j^2 &= \|p_A - p_i\|^2 - \|p_A - p_j\|^2 \\ &= (h_i - \delta_{ij})^2 - (h_j + \delta_{ij})^2 \\ &= h_i^2 - h_j^2 - 2\delta_{ij}(h_i + h_j) \\ &= (d_i^*)^2 - (d_j^*)^2 - 2\delta_{ij}d_{ij}^*. \end{aligned}$$

Then it follows that

$$\delta_{ij} = \frac{\left|\left(d_i^2 - d_j^2\right) - \left((d_i^*)^2 - (d_j^*)^2\right)\right|}{2d_{ij}^*}.$$

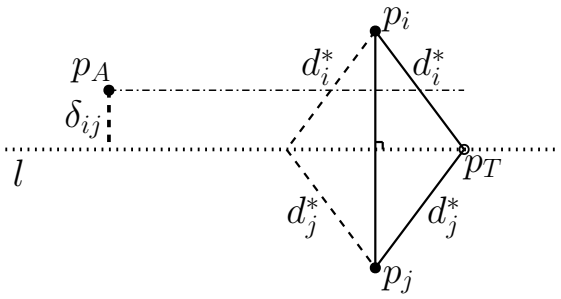

Figure 5: The radical axis l of the circles $C(p_i, d_i^*)$,$C(p_j, d_j^*)$.

Define $(N-1)$-dimensional vector

$$\delta(p_A) = \begin{bmatrix} \delta_{1N} \\ \vdots \\ \delta_{(N-1)N} \end{bmatrix}.$$

Note that $\delta(p_A)|_{p_A=p_T} = 0$. Lemma 2.2 of [21] implies that $\|\delta(p_A)\|^2$ is a convex function of p_A with global minimizer at $p_A = p_T$. Because d_{ij}^* is unknown to A, we consider the scaled distances

$$\xi_{ij} = \frac{\left|\left(d_i^2 - d_j^2\right) - \left((d_i^*)^2 - (d_j^*)^2\right)\right|}{2},$$

and

$$\zeta(p_A) = \frac{1}{N}\left\| \begin{bmatrix} \xi_{1N} \\ \vdots \\ \xi_{(N-1)N} \end{bmatrix} \right\|.$$

Similarly, Lemma 2.2 of [21] implies that $(\xi(p_A))^2$ is a convex function of p_A with global minimizer at $p_A = p_T$. Based on this fact, we propose the following algorithm:

$$v(t) = \begin{cases} \bar{v}, & \text{if } r_E(t) > \epsilon_r \\ 0, & \text{otherwise,} \end{cases} \tag{35}$$

$$\omega(t) = \begin{cases} \left((\mathrm{sgn}(\dot{\zeta}(t)) + 1)c + \dfrac{(1+\alpha)\bar{v}}{\zeta(t)}\right)\sigma\left(\dfrac{-\dot{\zeta}(t)}{\bar{v}}\right), & \text{if } \zeta(t) > \epsilon_r \\ 0, & \text{otherwise,} \end{cases} \tag{36}$$

where r_E is as in (27), and α, c are as in (9).

6. Simulations

In this section, we present the simulation results for the target capture and station keeping algorithms that we proposed in Section 2 and 5. We used MATLAB® with a fixed time step of 0.1 seconds for simulations. We set $c = 1$ in all simulations.

6.1. Target Capture

We analyzed the vehicle motion with the control law (5)-(8). The following parameter values were used in simulations:

$$\bar{v} = 0.3\text{m/sec}, \quad \epsilon_r = 0.3\text{m}.$$

The vehicle's initial and target locations were set as follows:

$$p_A(0) = [-3.2,\ 0.5]^\top \text{ m}, \quad p_T = [0,\ 0]^\top \text{ m}.$$

Fig. 6 represents the motion of the vehicle for different α and γ values for 30 seconds. Fig. 7 shows the range measurement r, the range rate $\dot{r}$, and the control signals v, ω. The vehicle achieved the objective successfully for all the parameter values given, i.e., the vehicle entered the $\mathcal{B}_{\epsilon_r}$ disc around the target T in a finite time (14 seconds) and stopped once it reached the disc. Difference in the parameters α and γ caused slight changes in the motion characteristics. Since ω is directly proportional to α, for the same γ setting, the higher α value (gray path) caused slightly sharper maneuvers compared with the lower α value (green path).

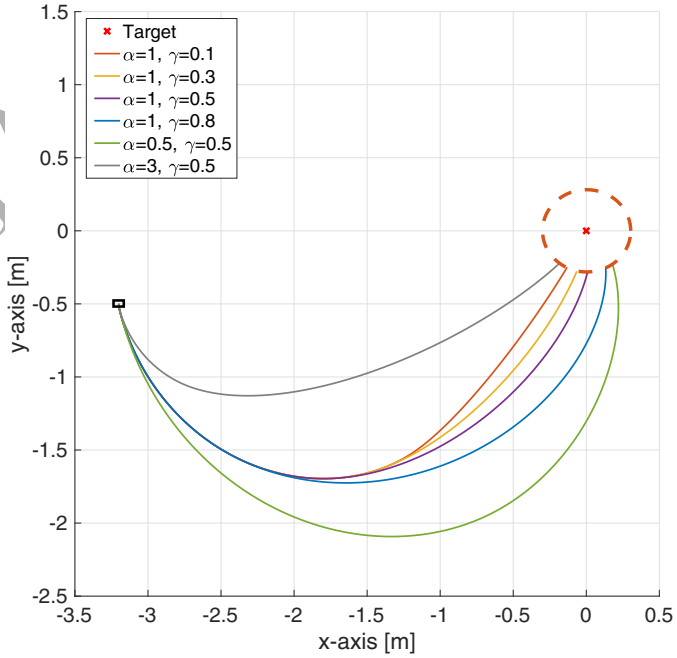

Figure 6: Target capture simulations: Vehicle motion on the plane with the control law (5)-(8). The black square and red cross denote the initial vehicle location $p_A(0)$ and the target location p_T, respectively.

6.2. Station Keeping

We now present the motion behavior of the vehicle with the control algorithms proposed in Section 5. We assumed that three beacons were located at the following positions:

$$p_1 = [-0.4,\ -0.2]^\top \text{ m}, \quad p_2 = [0.4,\ 0]^\top \text{ m}, \quad p_3 = [0,\ 0.5]^\top \text{ m}.$$

The target was located at $p_T = [0,\ 0]^\top$ m.

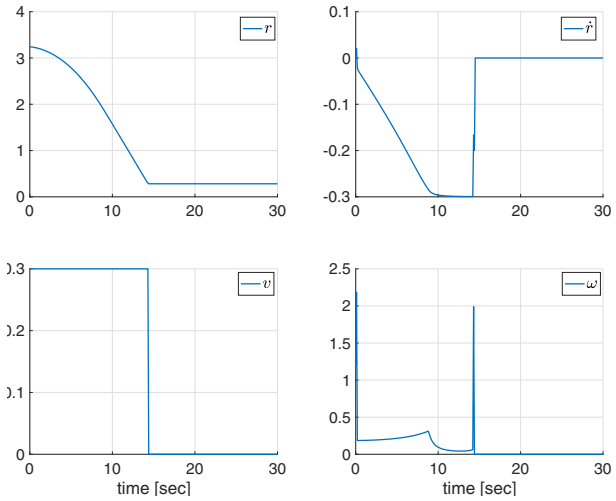

Figure 7: Target capture simulations: The range measurement r, time derivative of the range measurement $\dot{r}$, and the control signals v, ω.

We now present the performance of the control algorithm (32),(33) for different values of the design parameter k and the initial heading angle $\theta(0)$ (Fig. 8). Since k proportionally affects the magnitude of ω, higher k values produced sharper maneuvers for the same initial heading angle $\theta(0)$. For the same initial location and k setting, difference in the initial heading angle did not cause a significant change in the vehicle's trajectory.

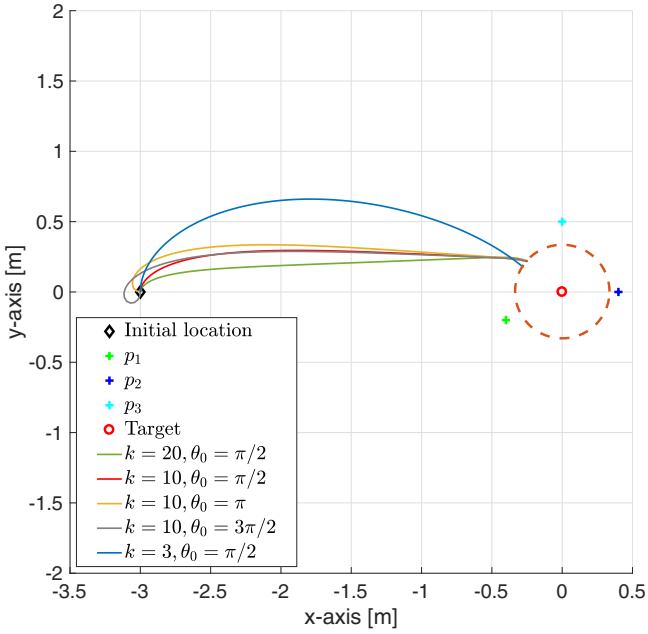

Figure 8: Station keeping based on circumnavigation simulations: Vehicle motion and positions of the beacons and the target.

Fig. 9 demonstrates the performances of the station keeping based on the inter-vehicle distance approach and station keeping based on convex cost function approaches for the same setting. The vehicle arrives the neighborhood $\mathcal{B}_{\epsilon_r}$ of the target in all runs. Station keeping based on convex function approach drives the vehicle to $\mathcal{B}_{\epsilon_r}$ in less time compared to the inter-vehicle distance regulation approach.

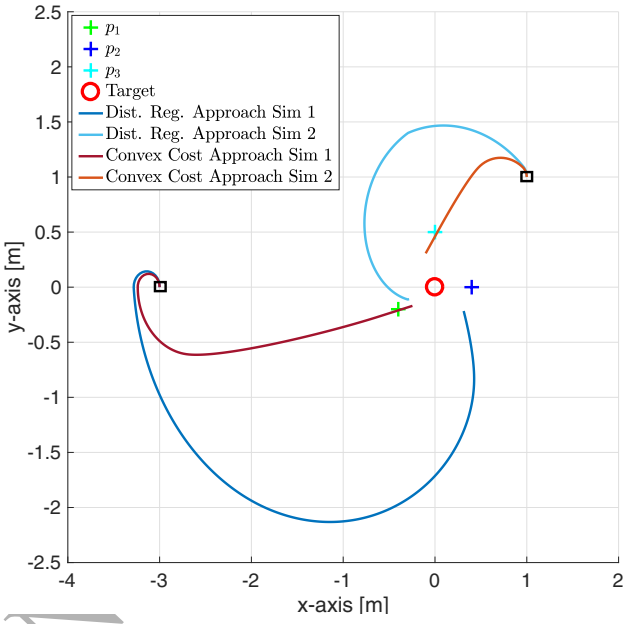

Figure 9: Station keeping simulations: Vehicle motion and positions of the beacons and the target. Black squares denote the initial locations.

7. Experiments

We evaluated our control algorithms with off-the-shelf ground robot and equipments.

7.1. Experimental Setup

We tested the control algorithms on an iRobot© Create ground robot (Fig. 10). iRobot has two actuated wheels on its two sides and one omnidirectional wheel on the front. This vehicle's motion is modeled by the nonholonomic kinematics (1). The vehicle accepts the linear speed v and angular speed ω as the control inputs, and converts them to the left and right wheel control inputs by the following relation:

$$v_l = v - \frac{l_{rad}}{2}\omega, \quad v_r = v + \frac{l_{rad}}{2}\omega, \tag{37}$$

where v_l, v_r are the control inputs for the left wheel and right wheel, respectively, and $l_{rad} = 252.5$mm is the distance between the left and right wheels.

We equipped the robot with an Odroid® microcontroller that runs the Robot Operating System (ROS). We used an Optitrack© Motive motion capture (Mocap) system to obtain the vehicle-target (or, for station keeping, vehicle-station) distance data to be used by the controller. The robot's ground truth position data were also obtained from the Mocap system for illustration purposes. The Mocap system was composed of 15 cameras that were mounted around the test area and connected

Figure 10: The iRobot© Create ground vehicle with Odroid (top) and the experimental testbed with Mocap cameras at the RISC Lab (bottom).

to a ground station. The Mocap system calculated the distance between the vehicle and the given virtual target (or, for station keeping, virtual stations) location, and transmitted it to the ROS environment. The Mocap system can generate accurate position data with up to few millimeters measurement errors. We calculated the range-rate data by using the first order difference between two consecutive range data as follows:

$$z[k] = \frac{r[k] - r[k-1]}{T_s},$$

where k is the time index, T_s is the sampling time, $r[k] = r(kT_s)$ is the range measurement at step k, and z is an approximation of the range-rate $\dot{r}$. Because the vehicle-target range data obtained from the Mocap system was precise, we obtained precise range-rate data by the first-order difference method in the experiments.

We note that the distance measurements can be obtained by other sensor fusion techniques applied to on-board sensors' data. One can also obtain the distance measurements by two ultrawideband (UWB) sensors, with one sensor being located at the target and with the other sensor being located on the vehicle.

7.2. Target Capture

We tested the target capture algorithm given in (5)-(8) for different parameter values. We used the same parameter values and initial conditions with the simulations for consistency. We located the target at $p_T = [0,\ 0]^\top$ m, and initiated the vehicle from $p_A(0) = [-3.2,\ -0.2]^\top$ m with the heading angle of $\theta(0) = 1.5\pi$ radians. In all experiments, fixed discrete step time of 0.1 seconds and the following parameter values were used:

$$\bar{v} = 0.3\text{m/sec}, \quad \epsilon_r = 0.3\text{m}, \quad c = 1. \tag{38}$$

iRobot's turning rate was being saturated at $\bar{\omega} = 4.25$rad/sec by the firmware. Thus, we selected the parameter α with respect to (9) as follows:

$$0 < \alpha < \frac{0.3(4.25 - 2)}{0.3} - 1 = 1.25.$$

However, we used $\alpha > 1.25$ in some runs to compare the performance.

We analyzed the motion behavior of the vehicle for different α and γ values (Fig. 11). The vehicle started from close locations with the same initial heading angle in all experiments. The vehicle achieved the objective in all experiments, i.e., it entered the $\mathcal{B}_{\epsilon_r}$ disc around the target in finite time (around 20 seconds) and stopped once it reached there. The algorithm with the parameter values $\alpha = 1$, $\gamma = 0.8$ showed the best performance in terms of path smoothness (blue path). For the other values of α, γ, the vehicle rotated a full turn at least once before it arrived the disc $\mathcal{B}_{\epsilon_r}$. We explain the reason for these full-turns in Section 7.4. Fig. 12 shows the range measurement r, the range rate $\dot{r}$, and the control signals v and ω for $\alpha = 1,\ \gamma = 0.1$.

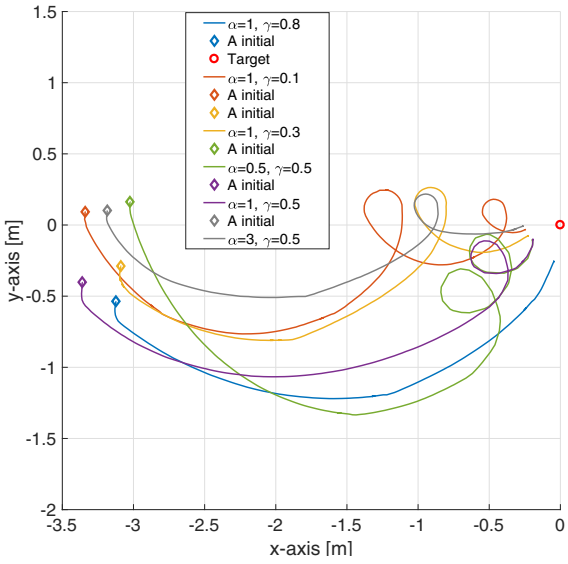

Figure 11: Target capture experiments: Trajectories of the vehicle for various α and γ values.

We repeated the target capture experiments with the sliding mode observer given in section 4 for $\gamma = 0.1$, $\alpha = 1$, and $k_1 = \{0.5, 1\}, k_2 = \{0.5, 1\}, k_3 = 0.1$. We observed that, for the same α, γ setting, the vehicle makes more full turns than the first-order difference method case and arrived the disc B_{ϵ_r} in 26 seconds for $k_1 = k_2 = 0.5, k_3 = 0.1$ and in 35 seconds for $k_1 = k_2 = 1, k_3 = 0.1$.

7.3. Station Keeping

Further, we evaluated performances of the three control algorithms presented in Section 5. In all experiments, we used three stations. We chose the positions of the stations randomly. We

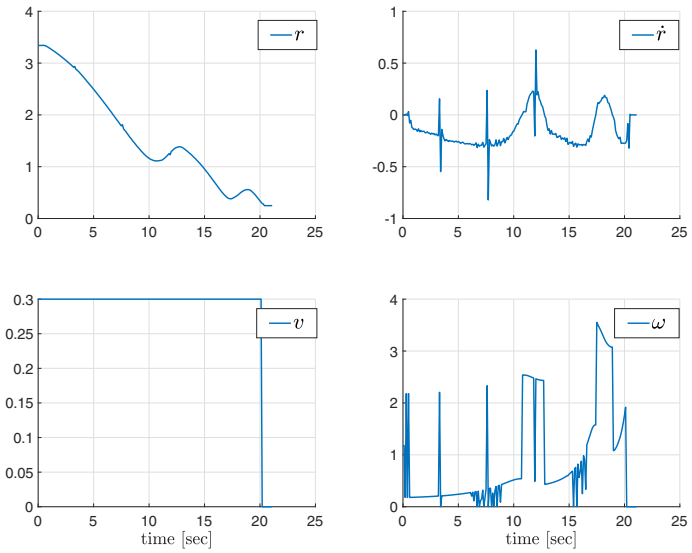

Figure 12: Target capture experiments: The range measurement r, the range rate $\dot{r}$, and the control signals v and ω for $\alpha = 1,\ \gamma = 0.1$.

used the following design parameter values in all experiment runs:

$$\bar{v} = 0.3\text{m/sec}, \quad \epsilon_r = 0.3\text{m}, \quad T_s = 0.1\text{sec}, \quad c = 1.$$

Station Keeping Based on Inter-Vehicle Distance Regulation: We tested the control law (30),(31) with three stations and the target being located at the following positions:

$$p_1 = [0.5,\ 0.2]^\top \text{ m},\ p_2 = [-0.6,\ -0.5]^\top \text{ m},\ p_3 = [0,\ 0.7]^\top \text{ m},\ p_T = [0,\ 0]^\top \text{ m}.$$

The vehicle's path for different α and γ values are shown in Fig. 13. Although the vehicle rotated full turn multiple times while searching for the target T, it entered the disc $\mathcal{B}_{\epsilon_r}$ around the target T in a finite time for all parameter values given.

Station Keeping Based on circumnavigation: We tested the algorithm (32),(33) with three stations and the target being located at the following positions:

$$p_1 = [0.5,\ 0]^\top \text{ m},\ p_2 = [0,\ -0.5]^\top \text{ m},\ p_3 = [-0.8,\ 0.1]^\top \text{ m},\ p_T = [0,\ 0]^\top \text{ m}.$$

The vehicle was initiated from different locations on the plane with different heading angles. The design parameter was set to $k = \{5, 10\}$. The vehicle arrived the disc $\mathcal{B}_{\epsilon_r}$ in all runs (Fig. 14). To analyze the effect of the parameter k to the path of the vehicle, we initiated the vehicle from two close locations with different k values (green and orange paths). We observed that the higher k value produced a smoother path compared to the lower k value.

Station Keeping Based on Convex Cost Function: We tested the algorithm (35),(36) with three stations and the target being

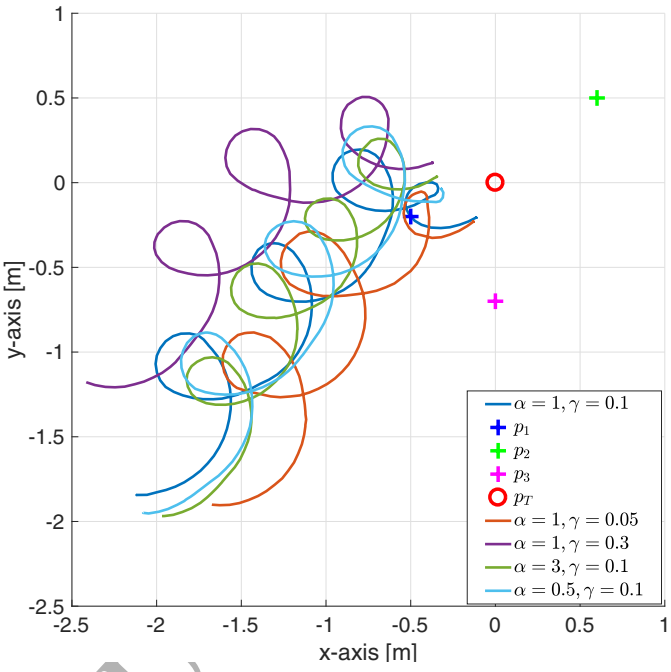

Figure 13: Station keeping based on inter-vehicle distance regulation experiment: Trajectories of the vehicle for various α and γ values and initial locations.

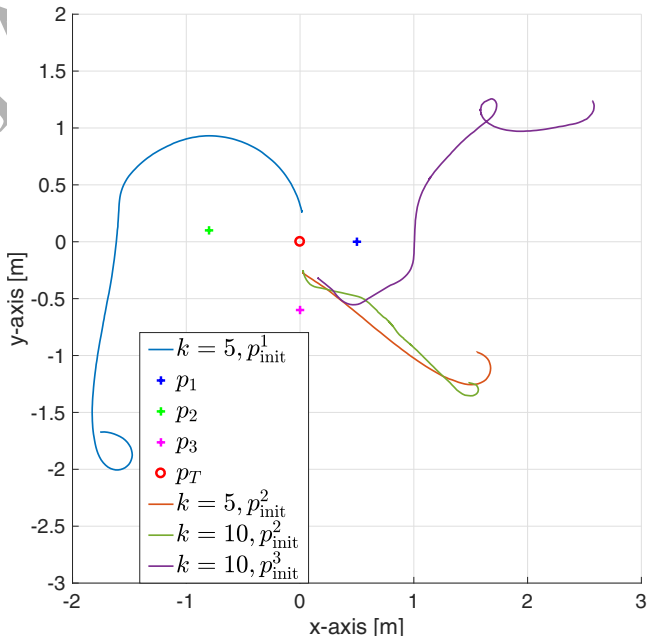

Figure 14: Station keeping based on circumnavigation experiment: Trajectories of the vehicle for various k values and initial locations.

located at the following positions:

$$p_1 = [0.5,\ 0]^\top \text{ m},\ p_2 = [0,\ -0.5]^\top \text{ m},\ p_3 = [-0.5,\ 0.0]^\top \text{ m},\ p_T = [0,\ 0]^\top \text{ m}.$$

We run the system for four different parameter sets (Fig. 15). We chose the vehicle's initial locations and heading angles to be very close to each other to compare the effects of the pa-

rameter values better. The vehicle arrived the disc $\mathcal{B}_{\epsilon_r}$ in three runs (blue, orange, and green paths) in finite times. In the other run (red path), since the vehicle had multiple full turn rotations while it was slightly approaching the target T, we ended the experiment before it arrived the target.

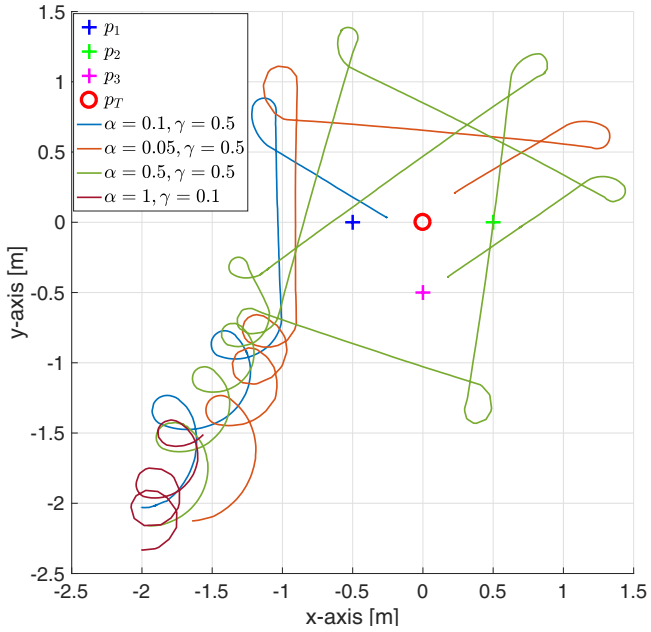

Figure 15: Station keeping based on convex cost function experiments: Trajectories of the vehicle for various α and γ values

7.4. Discussion on the Experimental Results

In this section, we demonstrate some of the experimental tests implemented to save space. We tested our control algorithms in much more experiments than what we illustrated in this section; for various vehicle initial locations, parameter values, and various target and station locations. The experiments verified the effectiveness and reliability of our target capture and station keeping algorithms. The differences between the simulation data and experiment data are the shape of the path driven by the vehicle toward the target and the time elapsed until the vehicle arrived the target. In target capture experiments, the most important factor that caused this difference is that the vehicle missed the equilibrium θ_{e1}, θ_{e2} in the experiments. Note that catching the actual equilibrium points θ_{e1}, θ_{e2} is usually not possible due to numerical properties of the hardware used. When θ_T lies in the interval $\frac{-\pi}{2} < \theta_T < 0$, θ_T starts approaching θ_{e2} which is very small for small γ values. While the robot approaches the equilibrium $\theta_T = \theta_{e2}$, θ_T became positive at times, and the robot had to rotate a full turn to enter again the equilibrium point in $\frac{-\pi}{2} < \theta_{e2} < 0$ (Fig. 3). This behavior can be seen in Fig. 11 where the vehicle had to rotate a full turn multiple times for $\gamma = \{0.1, 0.3, 0.5\}$. For instance, for $\gamma = 0.3$, $\alpha = 1$, we have $\theta_{e2} = -\sin^{-1}(0.15) \approxeq -0.15$rad, which is close to zero. Nevertheless, the vehicle-target distance decreased asymptotically and became less than the threshold ϵ_r after finite time. Since this issue did not occur in simulations, the simulation results were naturally much smoother. Another reason for the differences between the simulation and experimental results is the inaccuracies inherent to the robot's motion such as actuation dynamics. We note that despite these minor differences, both the simulations and experiments demonstrate the convergence property of our algorithms.

We set $c = 1$ in all our simulations and experiments. The design parameter c changes the time elapsed when the vehicle moves away from the target, i.e., when $|\theta_T| \geq \frac{\pi}{2}$, by adjusting the magnitude of ω. Since the parameter c, together with α, are related to $\bar{\omega}$ through (7), it can be chosen suitably to meet the maximum angular speed condition of a particular vehicle, if any. Specifically, if the actuation mechanism of the vehicle saturates the angular speed, the parameter c can be chosen in such a way that $\bar{\omega}$ does not exceed the saturation value. Thus, all properties of the proposed control laws will remain valid in the case of saturation nonlinearities.

In this section, we compared effects of different parameter values on a ground robot. The effects of these parameters may vary on a different robot because of the robot's individual dynamics. For this reason, we suggest tuning the parameters of our control algorithms experimentally for every robot within the bounds proposed here to find the best parameter setting for that individual robot.

8. Conclusion

We have proposed control algorithms for nonholonomic autonomous vehicle agents to solve target capture and station keeping problems. Our target capture algorithm requires only continuous agent-target range and range rate measurements. The station keeping algorithms require only continuous agent-beacon range and range rate measurements. We suggest the use of a sliding mode observer for the case where the range rate measurements are not directly available to the controller. We have presented the stability and convergence properties of the target capture algorithm and the station keeping based on circumnavigation algorithm. Furthermore, we have verified the applicability and effectiveness of the proposed algorithms on a ground robot in both simulations and experiments. Because our algorithms use only range and range rate measurements which can be obtained by UWB or by other low-cost range sensors, our algorithms can be used in GPS-denied environments or in scenarios where vision algorithms cannot provide enough information about the target.

Distance data obtained from range sensors usually include high noise. In future, we plan to analyze the stability and convergence properties under noisy range data. Additionally, we plan to implement the proposed algorithms on UAVs where the linear and angular velocities are not the actual control inputs, and the proposed algorithms need to be integrated with low-level motion controllers.

Acknowledgments

The research reported in this publication was supported in part by funding from King Abdullah University of Science and

Technology (KAUST). The work of B. Fidan is supported by the Canadian NSERC Discovery Grant 116806. The experiments were performed at the Robotics, Intelligent Systems, and Control (RISC) Laboratory, KAUST.

References

References

[1] J. Cochran and M. Krstic, "Nonholonomic source seeking with tuning of angular velocity," *IEEE Transactions on Automatic Control,* vol. 54, no. 4, pp. 717–731, 2009.

[2] B. Fidan, S. Dasgupta, and B.D.O. Anderson, "Adaptive range-measurement-based target pursuit," *International Journal of Adaptive Control and Signal Processing,* vol. 27, pp. 66–81, 2013.

[3] S. Dandach, B. Fidan, S.Dasgupta, and B.D.O. Anderson, "A continuous time linear adaptive source localization algorithm, robust to persistent drift," *Systems & Control Letters,* vol. 58, no. 1, pp. 7–16, 2009.

[4] B. Fidan, A. Çamlıca, and S. Güler, "Least-squares-based adaptive target localization by mobile distance measurement sensors," *International Journal of Adaptive Control and Signal Processing,* vol. 29, pp. 259–271, 2015.

[5] B. Fidan, S. Dasgupta, and B.D.O. Anderson, "Guaranteeing practical convergence in algorithms for sensor and source localization," *IEEE Transactions on Signal Processing,* vol. 56, no. 9, pp. 4458–4469, 2008.

[6] M. Deghat, I. Shames, B.D.O. Anderson, and C. Yu, "Localization and circumnavigation of a slowly moving target using bearing measurements," *IEEE Transactions on Automatic Control,* vol. 59, no. 8, pp. 2182–2188, 2014.

[7] T. Kim and T. Sugie, "Cooperative control for target-capturing task based on a cyclic pursuit strategy," *Automatica,* vol. 43, no. 8, pp. 1426–1431, 2007.

[8] I. Shames, S. Dasgupta, B. Fidan, and B.D.O. Anderson, "Circumnavigation using distance measurements under slow drift," *IEEE Transactions on Automatic Control,* vol. 57, no. 4, pp. 889–903, 2012.

[9] Y. Cao, "UAV circumnavigating an unknown target using range measurement and estimated range rate," in *2014 IEEE American Control Conference (ACC),* 2014, pp. 4581–4586.

[10] Y. Cao, "UAV circumnavigating an unknown target under a GPS-denied environment with range-only measurements," *Automatica,* vol. 55, pp. 150–158, 2015.

[11] A. Hashemi, Y. Cao, D. Casbeer, and G.Y. Yin, "UAV circumnavigation of an unknown target without location information using noisy range-based measurements," in *2014 IEEE American Control Conference (ACC),* pp. 4587,4592, 2014.

[12] M. Cao and A. S. Morse, "Station keeping in the plane with range-only measurements," in *2007 IEEE American Control Conference (ACC),* 2007.

[13] M. Cao and A. S. Morse, "An adaptive approach to the range-only station-keeping problem," *International Journal of Adaptive Control and Signal Processing,* vol. 26, pp. 757–777, 2012.

[14] B. Fidan, S. Dasgupta, and B.D.O. Anderson, "Realistic anchor positioning for sensor localization," in *Recent advances in learning and control,* V.D. Blondel, S.P. Boyd, and H. Kimura (ed.), Springer-Verlag, pp. 79–94.

[15] H.K. Khalil and J.W. Grizzle, *Nonlinear systems,* vol. 3. New Jersey: Prentice Hall, 1996.

[16] S. Güler, B. Fidan, S. Dasgupta, B.D.O. Anderson, and I. Shames, "Adaptive source localization based station keeping of autonomous vehicles," *IEEE Transactions on Automatic Control,* vol. 62, no. 7, pp. 3122–3135, 2017.

[17] J.A. Moreno and M. Osorio, "A Lyapunov approach to second-order sliding mode controllers and observers," in *2008 IEEE Conference on Decision and Control (CDC),* 2008, pp. 2856–2861.

[18] J.A. Moreno and M. Osorio, "Strict Lyapunov functions for the super-twisting algorithm," *IEEE Transactions on Automatic Control,* vol. 57, no. 4, pp. 1035-1040, 2012.

[19] S. Güler and B. Fidan, "Range based target capture and station keeping of nonholonomic vehicles without GPS," *2015 IEEE European Control Conference (ECC),* 2015, pp. 2970–2975.

[20] S. Güler, *Adaptive formation control of cooperative multi-vehicle systems,* PhD Thesis, University of Waterloo, 2015.

[21] B. Fidan and F. Kiraz, "On convexification of range measurement based sensor and source localization problems," *Ad Hoc Networks,* vol. 20, pp. 113–118, 2014.

[22] D. Milutinovic, D. Casbeer, Y. Cao, and D. Kingston, "Coordinate frame free Dubins vehicle circumnavigation using only range-based measurements," *International Journal of Robust and Nonlinear Control,* vol. 27, pp. 2937-2960, 2017.